



Semi-active vibration control of the motorized spindle using a self-powered SSDV technique: simulation and experimental study

Likang Zheng ^{a,b}, Ye He ^{a,b}, Lei Fan^{a,b}, Hongli Cao^c and Xiaoran Chen ^{a,b}

^aCollege of Mechanical and Vehicle Engineering, Chongqing University, Chongqing, People's Republic of China; ^bState Key Laboratory of Mechanical Transmission, Chongqing University, Chongqing, People's Republic of China; ^cCollege of Mechanical and Vehicle Engineering, Taiyuan University of Technology, Taiyuan, People's Republic of China

ABSTRACT

SSD (synchronized switch damping) is used for vibration control of the motorized spindle based on piezoelectric stack. Moreover, inspired by self-powered SSDI, a self-powered SSDV circuit was designed to overcome the disadvantages of requiring readjusting control parameters and sensor re-positioning of SSDI (synchronized switch damping on inductor) and SSDV (synchronized switch damping on voltage source). A simulation and an experimental were built, and the results show vibration control performance of self-powered SSDV is better than self-powered SSDI and is more flexible and effective than self-powered SSDI by adjusting the DC voltage to adapt to different speeds of the motorized spindle.

ARTICLE HISTORY

Received 23 June 2021
Accepted 7 March 2022

KEYWORDS

Semi-active vibration control; self-powered; synchronized switch damping on voltage; motorized spindle; piezoelectric shunt damping

1. Introduction

Vibration damping of engineering structures has received intensive attention and investigation in the last few years [1–3]. The previous conventional method of using damping materials has come to its limitation due to their poor tunability and low-frequency performance. It is more effective and flexible to use smart materials such as magnetorheological liquid [4] and shape memory alloy [5] for vibration suppressing of structures. The most promising one among these intelligent materials is piezoelectric materials because of its small size and broadband tunability [6,7]. Using piezoelectric material with an electrical network for damping vibration of structure is first proposed by Hagood [8]. Due to its high Curie temperature, good dielectric, ferroelectric, and piezoelectric properties, Lead Zirconate Titanate (PZT) is widely used in vibration active damping of some smart structures, such as smart cantilevered beam [9] and smart attitude and structural devices [10]. When the piezoelectric patch is connected with electrical elements, the vibration energy can be consumed by the resistor in the form of heat, which is the initial version of piezoelectric shunt damping (PSD) [11]. After that, considerably improved and optimized shunt circuits were designed, such as the parallel shunt [12–14], multimode shunt damping [15], and structure optimization [16–18]. Furthermore, to improve electromechanical conversion efficiency, the concept of negative capacitor [19] was introduced into PSD circuit, which

could overcome the inherent capacitive impedance of piezoelectric materials.

In addition to those passive ways, PSD also can function as semi-passive and semi-active vibration control methods. Typically, to broaden the frequency domain of passive vibration control and achieve better control results, a status switching method (SSD) was proposed by Richard and Clark [20,21]. Moreover, Richard [22] proposed the connecting resistance-inductance element to the two poles of the piezoelectric element, namely inductance synchronous switching damping (SSDI). Corr and Clark [23] obtained that the optimal closing time of SSDI switch is half of the period of the LC oscillating circuit composed of piezoelectric elements, capacitors, and inductors. These types of circuits are classified as semi-passive vibration control because no additional voltage or current sources are needed in the circuit. To further improve the turnover voltage across the piezoelectric energy-conversion element, Petit added a DC voltage source to the shunt circuits [24]. After that, Lefeuvre added two DC voltage sources to the shunt circuit, namely voltage-type synchronous switching damping (SSDV) [25]. Subsequently, Badel and Lallart found that when the reaction force generated by piezoelectric ceramics owing to the existence of inappropriate voltage sources is greater than the excitation force of the system, the system becomes unstable [26,27]. Therefore, an adaptive voltage source for the synchronized switching technique was proposed [26],

CONTACT Ye He  hifish2@gmail.com  College of Mechanical and Vehicle Engineering, Chongqing University, Chongqing 400044, People's Republic of China; State Key Laboratory of Mechanical Transmission, Chongqing University, Chongqing 400044, People's Republic of China

© 2022 The Author(s). Published by Informa UK Limited, trading as Taylor & Francis Group.

This is an Open Access article distributed under the terms of the Creative Commons Attribution License (<http://creativecommons.org/licenses/by/4.0/>), which permits unrestricted use, distribution, and reproduction in any medium, provided the original work is properly cited.

and a controllable DC voltage source was used to match the input excitation force. Other than adaptive SSDV, some other improved SSD techniques such as synchronized switch damping on negative capacitance and inductance (SSDNCI) [28,29] were continuously proposed.

In some applications based on SSD, it is relatively difficult to install additional sensors and controllers. By utilizing the electronic switch technique in the conventional SSDI control, Silva [30] proposed the self-powered synchronized switch damping on inductance (self-powered SSDI). Similarly, Shen et al. [31] realized simultaneous damping, sensing, and powering by using three piezoelectric transducers, and designed a low-power autonomous SSDV circuit with energy harvesting and management. To realize vibration damping with only one piezoelectric transducer, Lallart et al. developed a self-sensing SSDI composed of an envelope detector, comparator, and digital switch circuits [27]. Inspired by this technique, the self-sensing SSDV [32] and SSDNC [33] were proposed. From these studies, it is possible to realize a stand-alone system using SSD. Recently, Ji et al. [34] proposed unsymmetrical bipolar voltage with SSD based on a negative capacitance shunt circuit for vibration control.

Even though SSD has been widely investigated, it can be seen that most of them are applied to cantilevers or plates by attaching a piezoelectric patch to structures' surfaces. And SSD has never been applied to vibration control of motorized spindle up to now. The vibration of motorized spindle mainly comes from the rotor-bearing system. As an important component of high-speed machining (HSM), the vibration characteristics of the rotor-bearing system of the motorized spindle under various input conditions directly influence the dynamic performance of the motorized spindle. Considering the precision of manufacturing, it is certainly worthy of studying vibration control of this type of rotating structure. However, compared to those structures with flat surfaces, it is more difficult to apply piezoelectric transducers because geometrical complexity and high-speed rotation induce many difficulties for implementations. Although there are also some studies reporting vibration control of spindle using piezoelectric materials, most of them are based on active vibration control (AVC) [35–38]. The advantage of AVC is that the control effect is obvious, but the control algorithm is complex and adjusting parameters are difficult.

In this study, to overcome the control effect limitation of SSDI which is difficult to improve conversion efficiency owing to the quality of the inductor, a novel semi-active vibration control method, self-powered synchronized switch damping on voltage (self-powered SSDV), was proposed based on self-powered SSDI and applied to vibration control of motorized spindle. The self-powered SSDV improves the self-powered

SSDI and yields more flexibility, and further realizes semi-active vibration control based on PSD without sensors or controllers. It is well known that the excessive vibration of engineering structures tends to cause a failure of the bearings, which may cause an accident [39,40]. This method presented in this paper provides an idea of vibration reduction, so this method has potential engineering applications in vibration control of high-speed rotor-bearing systems.

The main contributions of this paper are as follows.

- (1) Self-powered SSDV was proposed, and the rotor-bearing system of motorized spindle was simulated. The results show that self-powered SSDV has obvious vibration control;
- (2) It is verified that self-powered SSDV has vibration control and is superior to self-powered SSDI in vibration control of motorized spindle;
- (3) SSD was applied to the vibration control of motorized spindle for the first time, and experiments were conducted for different speeds and supply voltages, which provide a novel idea and method for the vibration control of motorized spindle.

The paper is organized as follows: In Section 1, the vibration transmission model of motorized spindle was analyzed. In Section 2, a brief background of classic SSDI and SSDV was introduced to clarify the originality of the proposed novel SSD. Subsequently, the designed self-powered SSDV circuit was explained and its performance was compared to the self-powered SSDI from an angle of energy conversion. In Section 3, an electromechanical coupling simulation uses the single degree of freedom (SDOF) model designed in MATLAB/Simulink which demonstrates the theoretical analysis. After that, the rotor-bearing experimental platform was built to further verify and compare the vibration control performance of self-powered SSDI and SSDV in Section 4. Finally, some conclusions were drawn based on simulation and experimental results.

2. Theoretical analysis

2.1. Modeling of rotor-bearing system of motorized spindle

In motorized spindle, vibration mainly comes from rotor-bearing system. A schematic diagram of the rotor-bearing system is shown in Figure 1(a). To analyze the vibration transmission of the motorized spindle, the vibration transmission model of the motorized spindle in the vertical direction is shown in Figure 1(b). For the whole motorized spindle system, it can be simplified as mass, spring, and damping system. For the rolling element of the bearing, the mass of the rolling element is ignored, and the point contact between the raceway and the rolling element is assumed in this

paper. The motorized spindle vibration transmission model is composed of motorized spindle, bearing inner ring, bearing outer ring, and base. m_1 , m_2 , m_3 , and m_4 are the mass of motorized spindle, bearing inner ring, bearing outer ring, and base respectively. k_1 , k_2 , k_3 , and k_4 are the contact stiffness of the motorized spindle and the bearing inner ring in the vertical direction, the stiffness of the bearing in the vertical direction, the contact stiffness of the bearing outer ring, and the base in the vertical direction respectively. c_1 , c_2 , c_3 , and c_4 are the contact damping of the motorized spindle and the bearing inner ring in the vertical direction, the contact damping of the bearing in the vertical direction, the contact damping of the bearing outer ring and the base in the vertical direction, and the damping of the base in the vertical direction respectively. u_1 , u_2 , u_3 , and u_4 are the vibration displacement of motorized spindle, bearing inner ring, bearing outer ring and base in the vertical direction respectively. F_{ext} is the external force. F_p is the piezoelectric stacking force. Because the piezoelectric stack is made of piezoelectric ceramic flakes bonded by a special process, it can only withstand pressure.

The kinematic differential equation of motorized spindle is as follows:

$$F_{ext} - c_1(\dot{u}_1 - \dot{u}_2) - k_1(u_1 - u_2) = m_1\ddot{u}_1 \quad (1)$$

The kinematic differential equation of bearing inner ring is as follows:

$$c_1(\dot{u}_1 - \dot{u}_2) + k_1(u_1 - u_2) - c_2(\dot{u}_2 - \dot{u}_3) - k_2(u_2 - u_3) = m_2\ddot{u}_2 \quad (2)$$

The kinematic differential equation of bearing outer ring is as follows:

$$c_2(\dot{u}_2 - \dot{u}_3) + k_2(u_2 - u_3) - c_3(\dot{u}_3 - \dot{u}_4) - k_3(u_3 - u_4) = m_3\ddot{u}_3 \quad (3)$$

The kinematic differential equation of base is as follows:

$$c_3(\dot{u}_3 - \dot{u}_4) + k_3(u_3 - u_4) - c_4\dot{u}_4 - k_4u_4 - F_p = m_4\ddot{u}_4 \quad (4)$$

Equation (1) to Equation (4) were written together in matrix form, and the result is as follows:

$$M\ddot{u} + C\dot{u} + Ku = F_{ext} \quad (5)$$

where M is $\begin{bmatrix} m_1 & & & \\ & m_2 & & \\ & & m_3 & \\ & & & m_4 \end{bmatrix}$, C is $\begin{bmatrix} c_1 & -c_1 & & \\ -c_1 & c_1 + c_2 & -c_2 & \\ & -c_2 & c_2 + c_3 & -c_3 \\ & & -c_3 & c_3 + c_4 \end{bmatrix}$, K is $\begin{bmatrix} k_1 & -k_1 & & \\ -k_1 & k_1 + k_2 & -k_2 & \\ & -k_2 & k_2 + k_3 & -k_3 \\ & & -k_3 & k_3 + k_4 \end{bmatrix}$, F is $\begin{bmatrix} F_{ext} \\ 0 \\ 0 \\ -F_p \end{bmatrix}$, and u is $\begin{bmatrix} u_1 \\ u_2 \\ u_3 \\ u_4 \end{bmatrix}$. The external energy input of the motor-

ized spindle is generated by F_{ext} , and electromechanical conversion energy is generated by F_p . According to the kinematic differential equation of the rotor-bearing system, to achieve vibration control, the external input energy could be minimized by maximizing electromechanical conversion energy. The basic principle of SSD is to enhance the efficiency of conversion between mechanical and electrical energy for damping structural vibration.

In Figure 1, F_p is generated by piezoelectric stack. When an electric field is applied in the polarization direction of the piezoelectric stack, the dielectric deforms in a certain direction, which generates a force in the piezoelectric stack. It is because the piezoelectric stack deforms in the electric field that the force is

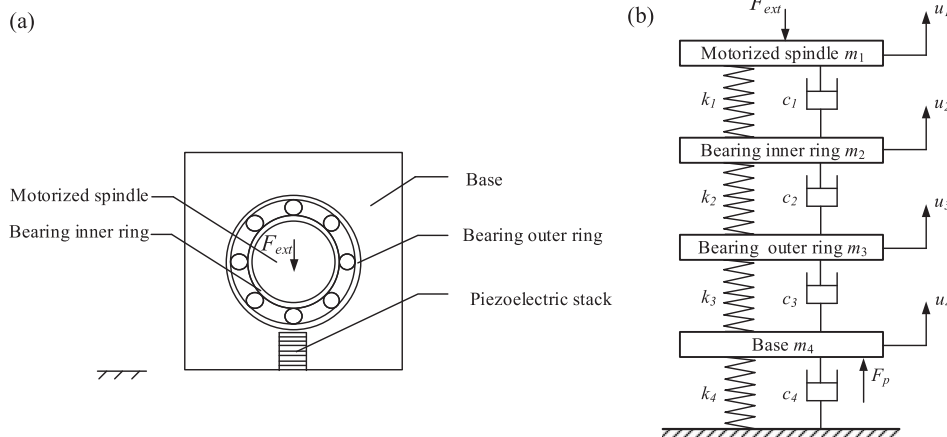


Figure 1. (a) Schematic of rotor-bearing system and (b) vibration transmission model of the motorized spindle.

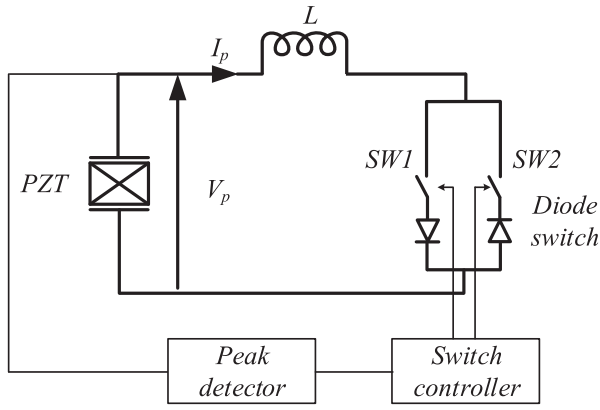


Figure 2. The schematic of classical SSDI control.

generated. This force meets electromechanical coupling Equation (6). When the electric field is removed, the force and deformation generated by the piezoelectric stack disappear.

$$\begin{cases} F_p = \alpha V_p \\ I = \alpha \dot{u} - C \dot{V}_p \end{cases} \quad (6)$$

where α is reaction factor coefficient, I and V_p are current and voltage across the stack, respectively. The reaction force coefficient α is related to the length and the cross-sectional area of the piezoelectric stack, and the piezoelectric constant.

2.2. Classic SSDI

Figure 2 shows the basic principle of SSDI. SSDI is a switching circuit. When the switch is switched on, the electrical boundary condition is electrical short circuit. When the switch is switched off, the electrical boundary condition is electrically open circuit. SSDV is also a switching circuit, so its electrical boundary condition is the same as SSDI. When the structural displacement reaches the maximum, closing the switch SW1 forms an oscillating circuit comprising the piezoelectric

ceramic C_p and inductor L . The closing time t_i is half the circuit cycle, and the voltage across the piezoelectric element changed from V_M to $-V_m$. The calculation of V_m is shown in Equation (8). V_M and V_m are the two peaks of the upper half of the piezoelectric patch voltage curve. When the voltage flip is completed, switch SW1 is switched off. When the structural displacement reaches the minimum, the closed switch SW2 changes the voltage on the piezoelectric element from $-V_M$ to V_m . The calculation of $-V_m$ is shown in Equation (9). This process enables the electromechanical energy conversion of the piezoelectric ceramic to be completed in one cycle. The variation curve of the voltage across the piezoelectric ceramic and the vibration displacement are shown in Figure 3.

$$t_i = \pi \sqrt{LC_p} \quad (7)$$

$$V_m = -V_M e^{-\pi/2Q_i} \quad (8)$$

$$-V_m = V_M e^{-\pi/2Q_i} \quad (9)$$

$$Q_i = \frac{1}{R} \sqrt{\frac{L}{C_p}} \quad (10)$$

The closing time of the circuit switch and the quality factor of the oscillating circuit are shown in Equations (7) and (10). Equation (10) shows that the quality factor of the oscillating circuit Q_i is inversely proportional to the resistance R . Therefore, the total series resistance of the circuit affects the output voltage amplitude.

2.3. Classic SSDV

To further enhance the turnover voltage across the piezoelectric ceramic, Lefevre [25] connected two DC voltage sources V_C on the branch of SSDI, namely SSDV, which enhances the effect of voltage flipping. Figure 4 shows the conventional SSDV control, and the control strategy of the SSDV circuit is the same

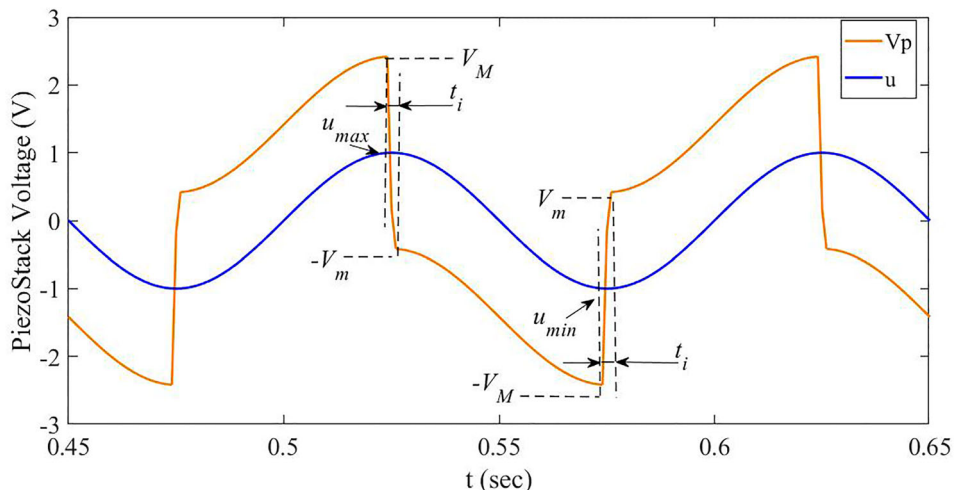


Figure 3. Piezoelectric patch voltage and the structural displacement of SSDI.

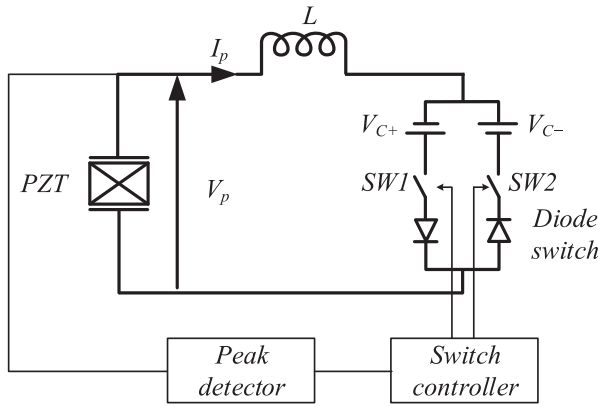


Figure 4. The schematic of classic SSDV control.

as that of SSDI. When the switch SW1 is closed, the voltage across the piezoelectric ceramic changes from V_M to $-V_m$ instantaneously, and the equation of V_m is shown in Equation (11). At the closing moment of the switch SW2, the voltage at both ends of piezoelectric ceramics changes from $-V_M$ to V_m , and the equation of V_m is shown in Equation (12). The variation curves of the voltage across the piezoelectric ceramic and the vibration displacement are shown in Figure 5.

$$-V_m = -(V_M + V_C)e^{-\pi/2Q_i} - V_C \quad (11)$$

$$V_m = (V_C - V_M)e^{-\pi/2Q_i} + V_C \quad (12)$$

2.4. Comparison of SSDI and SSDV

The proposed self-powered SSDV was inspired by the higher conversion efficiency of SSDV in comparison

with SSDI circuit. Hence, these two circuits from an angle of energy conversion were analyzed and compared. The energy transmitted by the piezoelectric element and electric networks can reflect the control effect directly. The energy transmitted by the piezoelectric ceramic is the integral of the output voltage and the vibration displacement of the circuit, which is expressed in Equation (13).

$$\int \alpha V_p \dot{u} dt = \int \alpha V_p du \quad (13)$$

Figures 6 and 7 are the comparisons of voltage output and transmitted energy cycles between SSDI and SSDV circuits respectively. The figures show that the output voltage across the piezoelectric element in the SSDV circuit is higher than that of SSDI. The two vertical lines in the transmitted energy cycles of Figure 7 are the voltage turnover process of the piezoelectric ceramic during the closing time of the switch, and the two oblique lines indicate that the voltage across the circuit is proportional to the vibration displacement when the circuit is open. The energy transmitted by the SSDI and SSDV control can be determined by calculating the area of the rectangle, whose equation is shown in Equation (14). Based on Equations (8) and (9), the energy consumed by SSDI is a function of the displacement u , whose equation is shown in Equation (15). As indicated by Equations (11) and (12), the energy consumed by SSDV is a function of displacement u and voltage V_C , whose equation is shown in Equation (16).

Equations (8) and (12) show that the SSDV circuit has one more turnover voltage amplitude

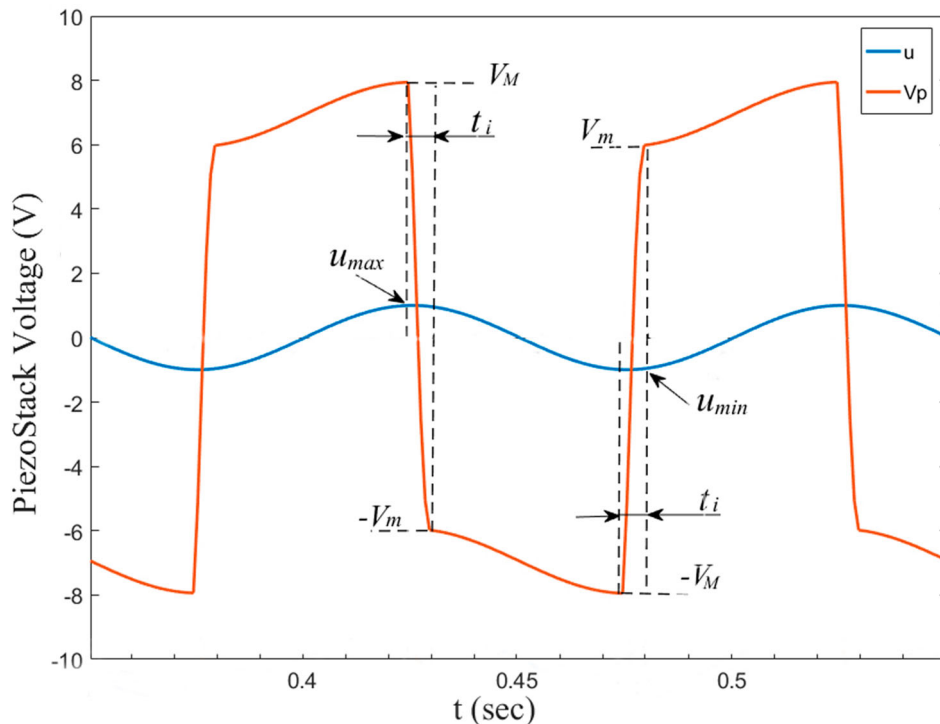


Figure 5. Piezoelectric patch voltage and the structural displacement of SSDV.

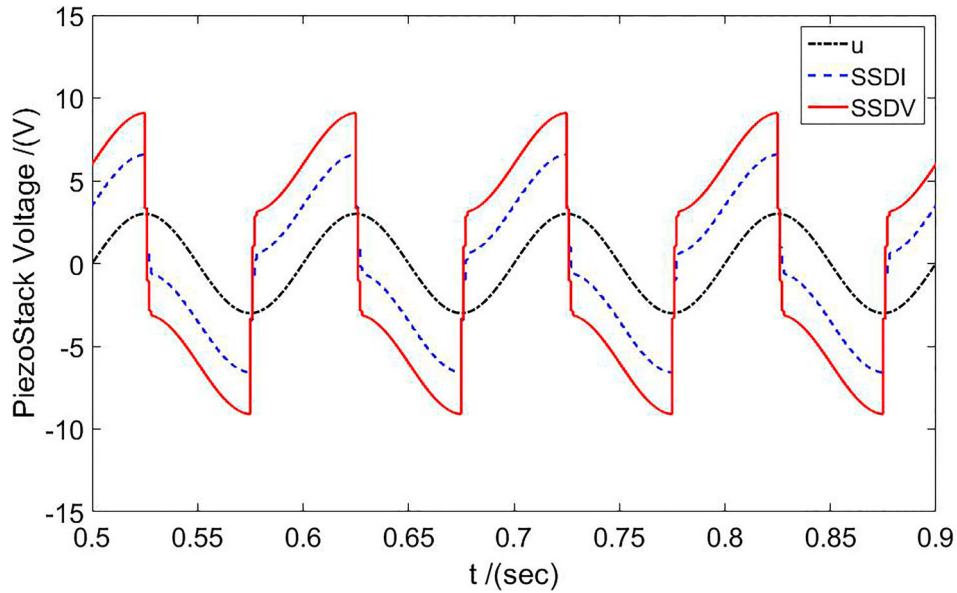


Figure 6. Voltage outputs of the SSDI and SSDV circuits.

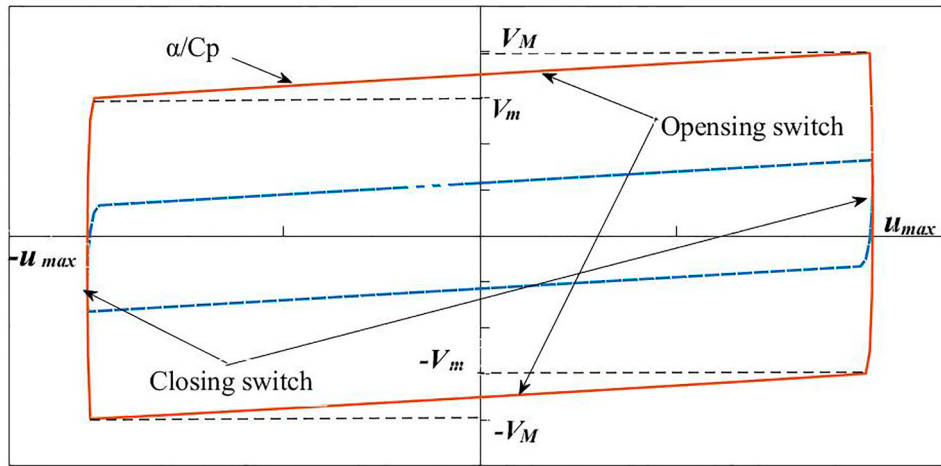


Figure 7. Transmitted energy cycles of the SSDI and SSDV.

$(1 + e^{-\pi/2Q_i})V_C$ than SSDI circuit. In other words, the voltage source V_C directly increases the flip voltage between the two ends of piezoelectric ceramics. As implied by Equations (15) and (16) within one cycle, the SSDV circuit converts more energy than the SSDI circuit. Therefore, it is expected that SSDV can offer a better damping effect.

$$\int_0^T \alpha V du = 2\alpha u_m (V_M + V_m) \quad (14)$$

$$\int_{SSDI}^T \alpha V du = \left(4 \frac{\alpha^2}{C_p} u_m^2\right) \frac{1 + e^{-\pi/2Q_i}}{1 - e^{-\pi/2Q_i}} \quad (15)$$

$$\int_{SSDV}^T \alpha V du = \left(4 \frac{\alpha^2}{C_p} u_m^2 + 4\alpha u_m V_C\right) \frac{1 + e^{-\pi/2Q_i}}{1 - e^{-\pi/2Q_i}} \quad (16)$$

2.5. Self-powered SSDV

Conventional SSDV switch control requires the measured vibration displacement or velocity of the structure

as the control signal. To measure the amplitude variation of the piezoelectric ceramic in a spindle system, a displacement sensor needs to be installed in a small space accurately, which is difficult in real engineering. If the displacement sensor is installed in a different location deviating from the piezoelectric ceramic stack, the wave peak or trough measured by the displacement sensor may not necessarily coincide with the one of piezoelectric ceramic stack because of geometric error in the machining of the spindle profile. Consequently, the SSDV controller might not work effectively. To achieve the synchronized switch technique in environmental vibration energy harvesting, an analogic switch was used to automatically control the synchronized switch in synchronized switching harvesting on inductor (SSHI) according to the variation of the output voltage across the piezoelectric element [41,42]. Furthermore, automatic switch control was proposed in the conventional SSDI control [30].

However, as mentioned in the previous section, there is a limitation of control effect for SSDI damping

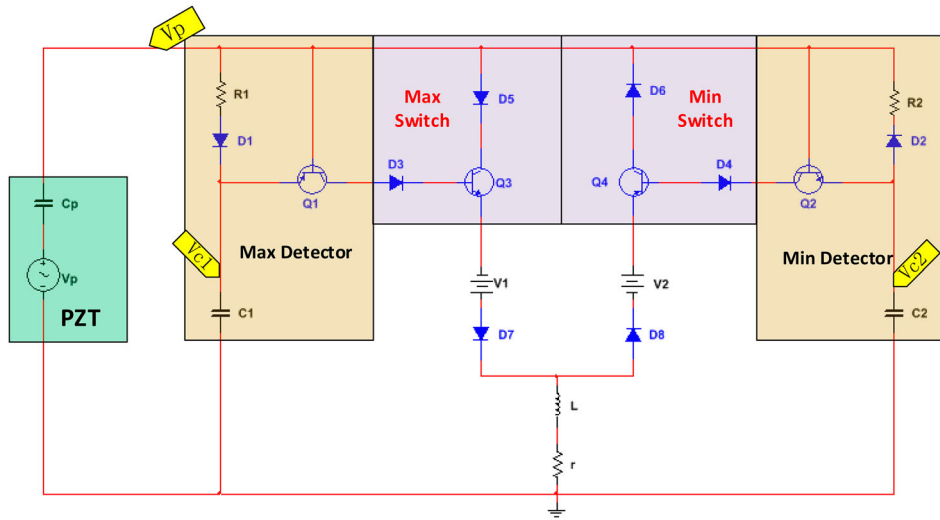


Figure 8. Circuit design of self-powered SSDV.

Table 1. Self-powered SSDV circuit parameters.

Symbol	Quantity	Parameter
C_p	PZT capacitor	2 F ($\pm 20\%$)
$R_{ed}(R_1, R_2)$	Charging resistance	1 k Ω
$C_{ed}(C_1, C_2)$	Charging capacitance	100 nF
D1–D8	Diode	1N4007
Q1–Q4	PNP transistor	TIP42C and TIP41C
L	Inductance	200 mH
R	Resistance moment	300 Ω
V1, V2	DC power supply	(3,6,9,12) V

technique. To improve the performance of the synchronized switch, self-powered SSDV was proposed based on self-powered SSDI. In the self-powered SSDV, two additional external DC voltage sources were connected in series with the switch, directly increasing the turnover voltage of piezoelectric ceramic stack.

The self-powered SSDV circuit is shown in Figure 8, where V_p is the voltage across the piezoelectric ceramic stack, and V_{C1} and V_{C2} is the voltage across the capacitor C_1 and C_2 respectively. In the self-powered SSDV circuit, a pair of complementary transistor topological structures were used for the direct envelope detection of the voltage V_p across the piezoelectric stack. In other words, the structures were used to detect the maximum and minimum voltage of the piezoelectric ceramic through the Max Detector module and the Min Detector module respectively. Another pair of complementary transistor topological structures were applied as the Max Switch and Min Switch of the output voltage across the piezoelectric stack respectively. The external DC voltage sources V_1 and V_2 in Figure 8 are the maximum and minimum loop voltage sources respectively. The main parameters of the circuit are shown in Table 1. Because of the lack of theoretical support for the appropriate voltage source matching problems, some trial-and-error experiments were used to find the appropriate voltage source. The result implies that voltages can be selected in the range from 3 V to 12 V.

As can be seen from Figure 9, during the positive half-cycle, when the structure is subjected to an external exciting force and the circuit is opened, voltage V_p is generated across the piezoelectric ceramic stack and V_p charges the piezoelectric ceramic capacitor C_p as well as the circuit capacitors C_1 and C_2 . When the vibration displacement gradually increases to the maximum value, the voltage V_p across the piezoelectric ceramic, V_{C1} and V_{C2} across the capacitors also reach the maximum value V_{max} . As the vibration displacement gradually decreases, V_p , V_{C1} , and V_{C2} decrease at the same time. Because the capacitor is capable of retaining the voltage to some extent, V_{C1} and V_{C2} would not drop as rapidly as V_p . Therefore, when the difference between V_{C1} and V_p is greater than $V_D + V_{BE}$ (the threshold voltage across the triode and the diode), the switch of the triode Q_3 is closed to connect the circuit, and the left half of the circuit completes voltage turnover at the maximum displacement. Similarly, in the negative half-cycle, when the difference between V_p and V_{C2} reaches the threshold voltage across the triode and the diode ($V_D + V_{BE}$), the switch of the triode Q_4 is closed to connect the circuit and the right half of the circuit completes the voltage turnover at the minimum displacement.

The entire process of voltage turnover is performed as mentioned above. To ensure that the circuit can run normally, the following two requirements should be met:

- (1) The peak voltage output of the piezoelectric ceramic has to be greater than the threshold voltage of the diode and the triode:

$$V_{p\max} = \frac{\alpha}{C_p} u_m > V_{CE(sat)} + 3V_D + V_{BE} \quad (17)$$

where $V_{CE(sat)}$ is the saturation voltage of the collector–emitter of the triode, V_{BE} is the break-over voltage of the base-emitter of the triode, and V_D is

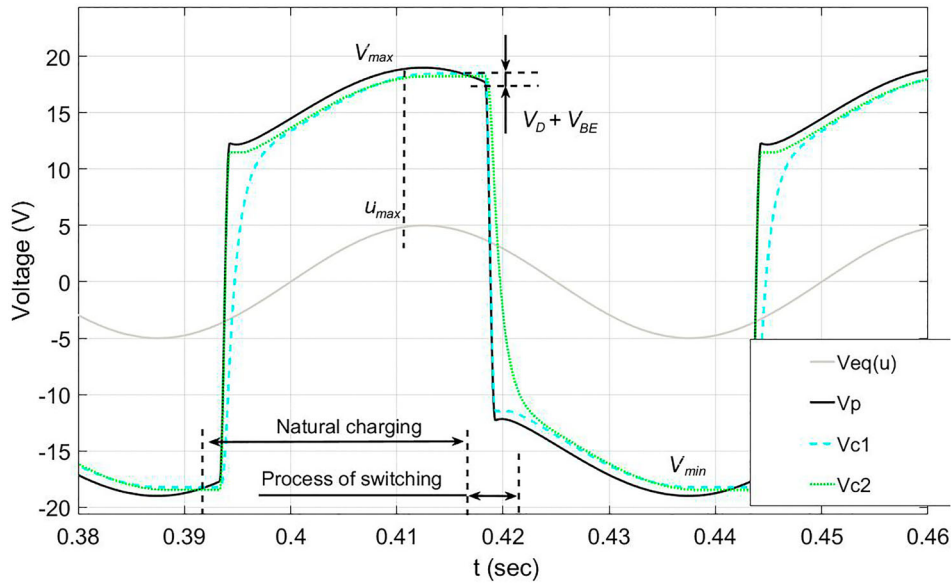


Figure 9. Piezoelectric patch voltage and the structural displacement of self-powered SSDV.

the break-over voltage of the diode. Table 2 shows the parameters of the triode and the diode.

- (2) Only appropriate C_1 and C_2 can power the switching triode, which requires a continuous process of trial and experimental modification. However, C_1 and C_2 need to meet the following equation [41]:

$$2\pi\sqrt{LC_p} < R_{ed}C_{ed} \ll \pi/\omega \quad (18)$$

where ω is the exciting frequency of the mechanical system, π/ω is half of the vibration cycle of the mechanical system, $R_{ed}C_{ed}$ is the charging time of the capacitance, and $2\pi\sqrt{LC_p}$ is the oscillation cycle of the circuit. The first inequality, the charging time of the capacitor, is longer than the oscillation cycle of the circuit. Consequently, voltage turnover should be faster than the time needed to charge the capacitor, to prevent the circuit switch from misjudging when the maximum or minimum displacement is reached. The second inequality shows that the time charging the capacitor is less than half the circuit's vibration cycle. Consequently, the capacitor is fully charged to power the switch when the vibration displacement reaches its peak.

3. Simulation study

3.1. Electromechanical coupling simulation model

When analyzing the vibration control of self-powered SSDI and self-powered SSDV, the motorized spindle system can be regarded as an SDOF model. In this section, the electromechanical coupling simulation based on the SDOF model along with self-powered SSD circuit was established to demonstrate the theoretical analysis. It is convenient and effective to use the

Table 2. Transistor parameters in the circuit.

Symbol	Quantity	Value
V_D	Diode forward voltage drop	0.6V
V_{BE}	Transistor base-emitter on voltage	0.5V
$V_{CE(sat)}$	Transistor collector-emitter on voltage	1.2V

MATLAB/Simulink's internal piezoelectric stack module (shown in Figure 10) where related mechanical and electrical parameters are complete enough to simulate a real device for conducting the simulation. Although there certainly exists a discrepancy between the idealized SDOF model with rotor-bearing system, it can be still regarded as theoretical support. Furthermore, in the following experiment, Both eccentric loads and response points are closed to the position of bearing so that it meets the dynamic condition displayed in the SDOF model as possible.

Figure 10 shows the electromechanical coupling simulation model of self-powered SSDI and self-powered SSDV established in MATLAB/Simulink. This model is a mechanical system consisting of the equivalent mass block, spring, and damping block simulating the bearing and piezoelectric stack. On the right is the self-powered control circuit, where SW1 controls the turn-on time of the circuit and SW2 decides whether the circuit is controlled by self-powered SSDI or self-powered SSDV. The input of the system is a harmonic exciting force $F = 300 \sin(50 \cdot 2\pi t)$, and the outputs of the system are the voltage across the piezoelectric stack and the displacement of the mass block.

3.2. Results and discussion

In the vibration damping simulation of the equivalent rotor-bearing system with a piezoelectric stack, when the charging capacitors C1 and C2 reach a certain

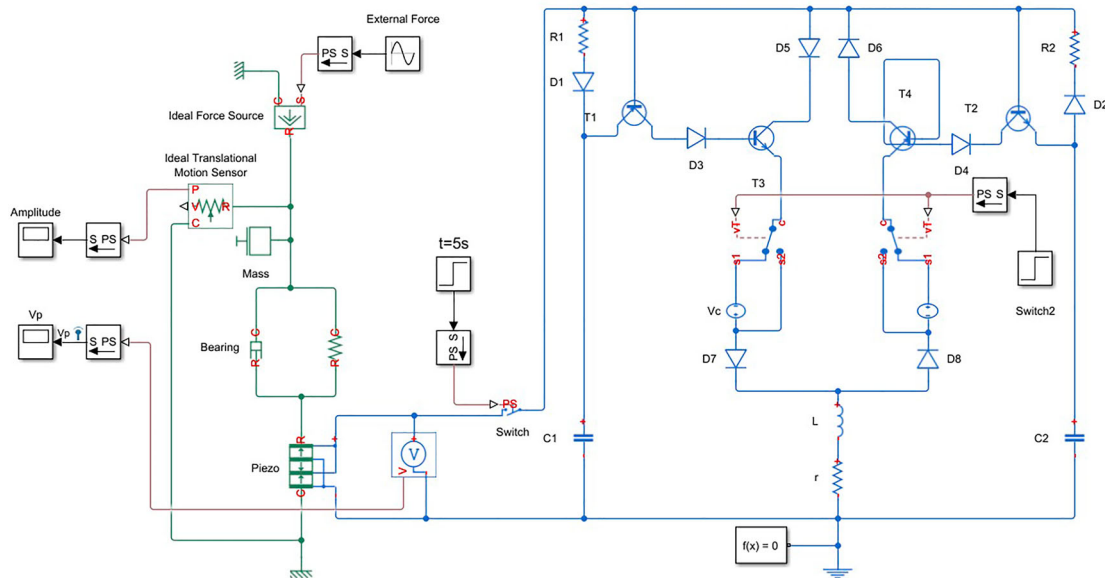


Figure 10. Electromechanical simulation model in MATLAB/Simulink.

voltage value, transistors T3 and T4 can be powered and the control circuit can function. Figure 11(a) and (b) show the voltage across the piezoelectric stack and the first-order vibration amplitude of the mass for self-powered SSDI and self-powered SSDV respectively. Before the switch is closed, the voltage across the piezoelectric stack is proportional to the vibration displacement of the system, and both voltage and vibration displacement decrease gradually because of the mechanical damping of the system. When the switch is closed, the output voltage across the piezoelectric ceramic increases and the vibration amplitude of the mass decreases. In the simulation, the self-powered SSDI reduces the vibration amplitude of the rotor by 0.11×10^{-6} m and the vibration quantity by 5.1%, while the self-powered SSDV method reduces the vibration amplitude of the rotor by 0.39×10^{-6} m and the vibration quantity by 18.4%.

The self-powered SSDI cannot effectively damp the rotor's vibration mainly because the circuit loss and part of the consumed threshold voltage of the transistor lead to an unsatisfactory voltage turnover and reduce the electromechanical coupling coefficient of the rotor-bearing system, as shown by the inset of Figure 11(a). Because self-powered SSDV can provide the voltage source, it can overcome the circuit loss and transistor voltage. Therefore, the voltage turnover is more ideal. As shown by the inset of Figure 11(b), although the turnover does not occur at the displacement peak, the damping effect is not affected.

4. Experimental investigation

4.1. Experimental setup

In the simulation results, the vibration control performance of self-powered SSDV is better than that of

self-powered SSDI. To further test the vibration control performance of the proposed circuit, an experiment was carried out on the vibration control of motorized spindle, where the circuit design and parameter selection refer to the simulation. Figure 12(a) and (b) display the schematic and physical platform of the semi-active vibration control system with piezoelectric shunt damping methods for the motorized spindle based on self-powered SSDV respectively. The spindle speed was controlled by the upper computer sending instructions to the motor driver, the eccentric mass disc was installed at the loading end, and the spindle bearings were supported with the piezoelectric stack. When the spindle rotates, the vibration energy of the rotor-bearing system was converted into electric energy through the piezoelectric stack, and the vibration control is performed through the connection with a self-powered SSD circuit. In the experiment of the self-powered SSDI, the spindle rotating speeds were 2000, 3000, and 4000 r/min respectively. For the self-powered SSDV, its control voltages were 3, 6, 9, and 12 V respectively. And the experimental rotating speeds were 3000, 4000, and 4500 r/min, respectively. The vibration amplitude of the spindle was obtained by installing an eddy current displacement sensor close to the bearing, which is shown in Figure 12.

4.2. Experimental results

Figure 13 shows the time-domain and frequency-domain (Fast Fourier Transform) vibration amplitude of the motorized spindle under self-powered SSDI and self-powered SSDV when the rotating speed of the spindle rotor is 3000 r/min. With self-powered SSDI, the vibration amplitude of the spindle is reduced 0.09×10^{-6} m at a percentage of 3.8% while

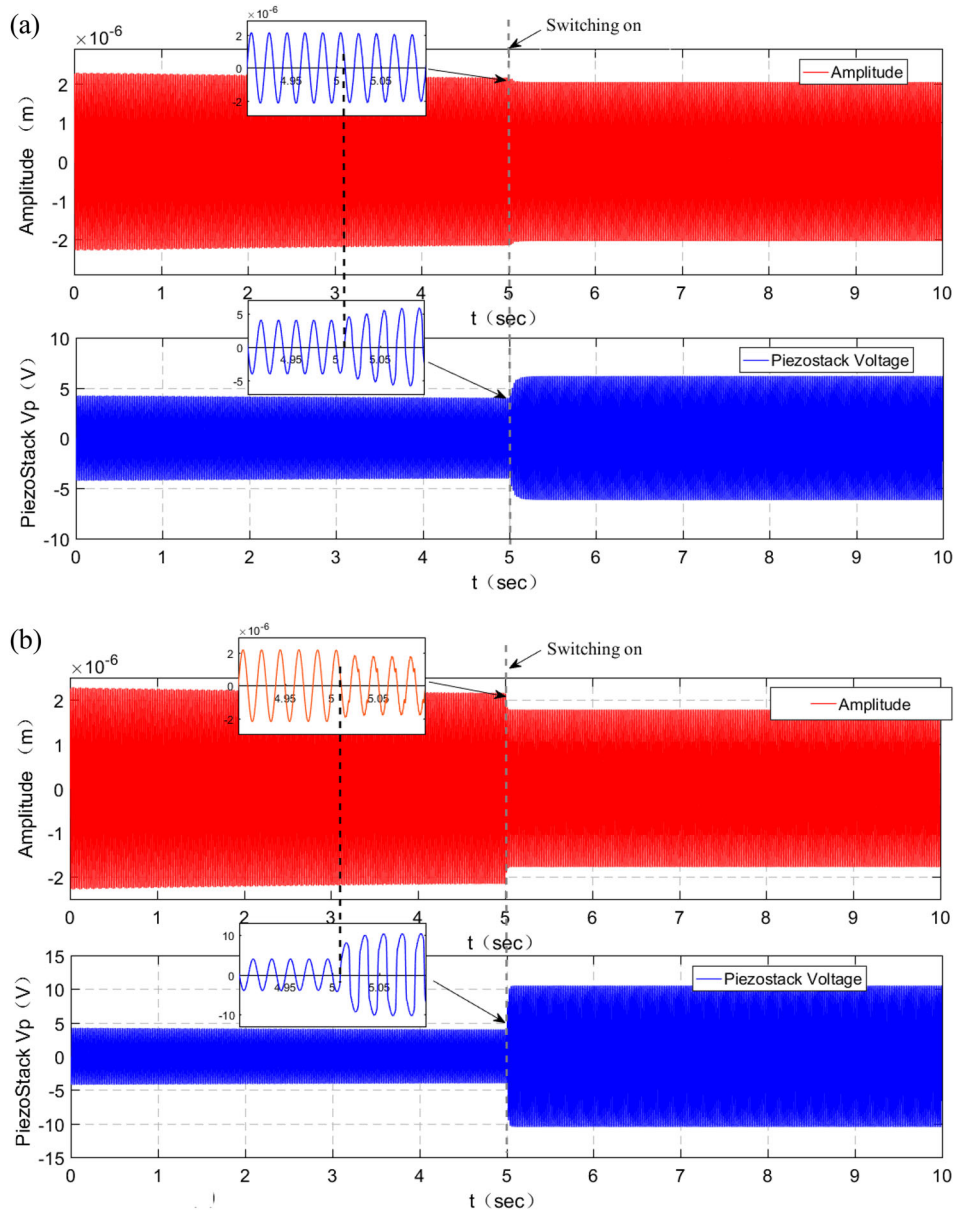


Figure 11. Vibration-damping effect: (a) Self-powered SSDI (b) Self-powered SSDV.

self-powered SSDV reduces the vibration amplitude of the spindle by 0.17×10^{-6} m at a percentage of 7.1%. The experimental results show the self-powered SSDV has a better vibration control performance on the rotor-bearing system than self-powered SSDI.

Figure 14 compares the vibration control effects of self-powered SSDI and self-powered SSDV under different rotating speeds of the motorized spindle. As the rotating speed of the spindle increases, due to the eccentric load, the vibration amplitude of the spindle increases correspondingly and the performance of SSDI declines. When the rotating speed is within the range of 3000–4500 r/min, the overall vibration control effect of self-powered SSDV with supply voltage 3–12 V is always superior by 1–50% to that of self-powered SSDI. The control effect of self-powered SSDV can be changed with different voltage sources. When the voltage is set at 9 V, self-powered SSDV offers the best control

effect, reducing the vibration amplitude of the spindle rotor by about $0.3 \mu\text{m}$, and the vibration decreases by about 13%. Notably, it should be pointed out that the weaker control performance with voltage 12 V than that with 9 V is attributed to the instability of higher voltage, which might bring additional adverse vibration for structure. This phenomenon was explained in detail in Ref. [27]. Thus, for SSDV vibration control, the selection of voltage is vitally important. Because SSDV has no self-adaptive function, the trial-and-error method was used to choose suitable voltage and avoid instability.

4.3. Analysis and discussion

From the measured results, it can be seen that self-powered SSDV has a significant performance on vibration control of motorized spindle. And compared

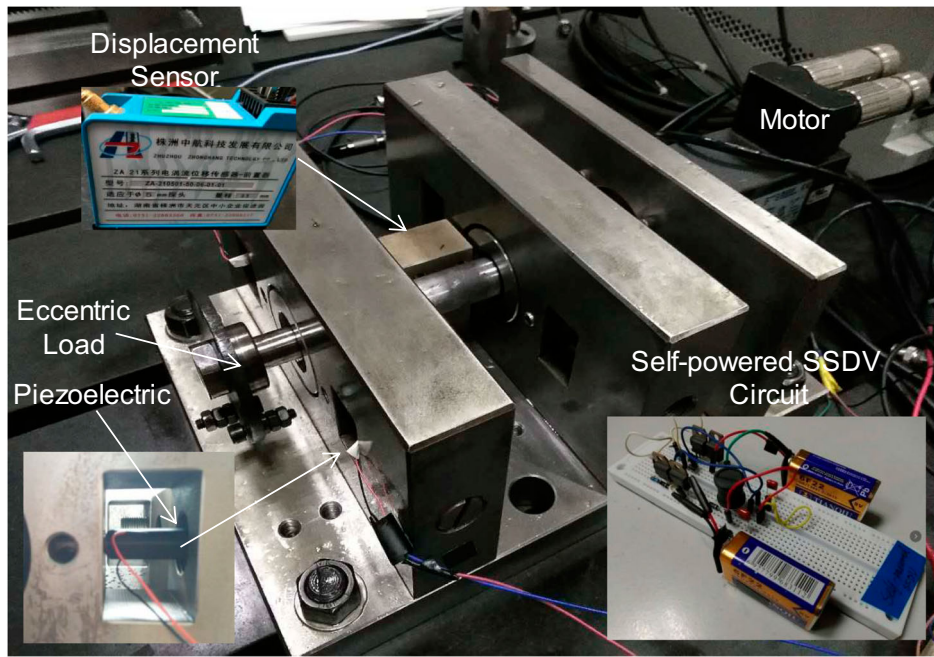
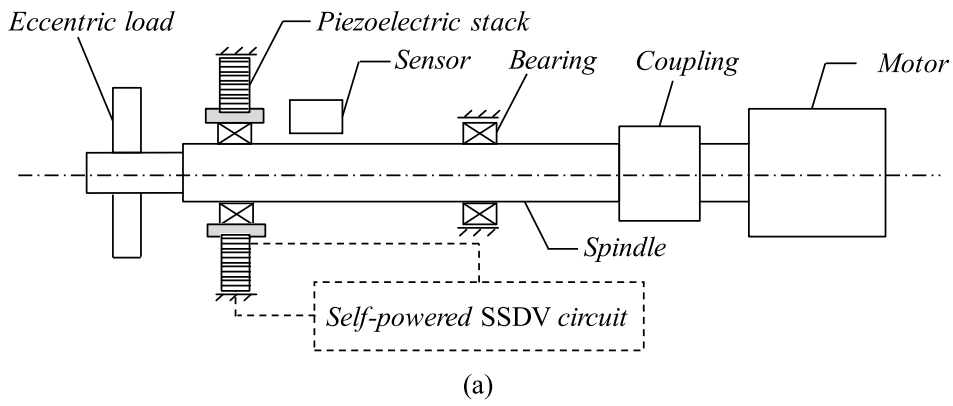


Figure 12. (a) Schematic (b) Experimental rotor-bearing setup.

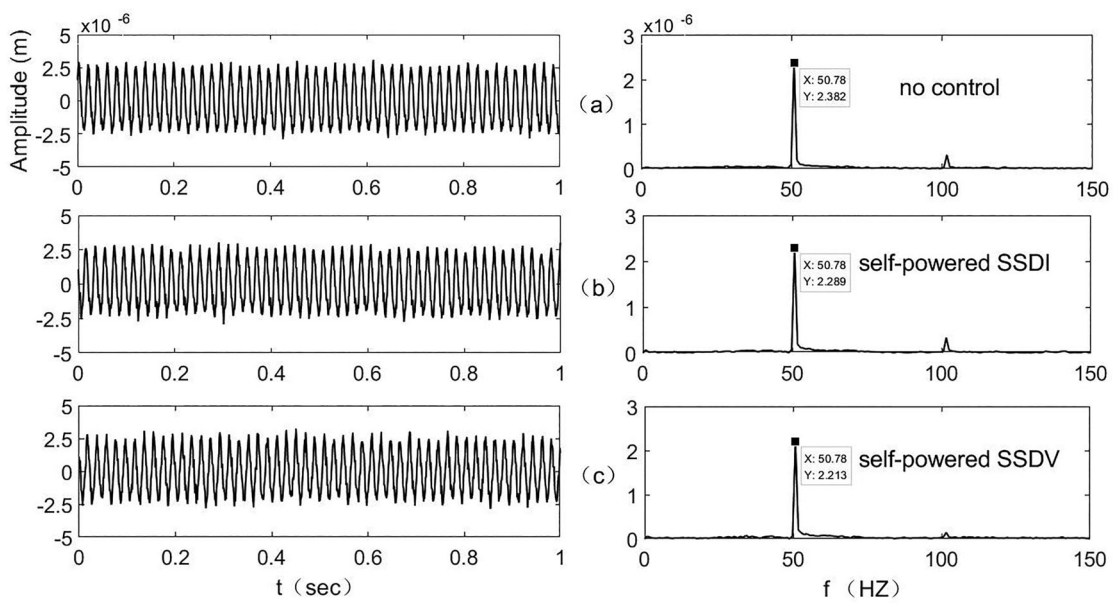


Figure 13. Vibration control comparison: (a) No vibration control (b) Self-powered SSDI (c) Self-powered SSDV.

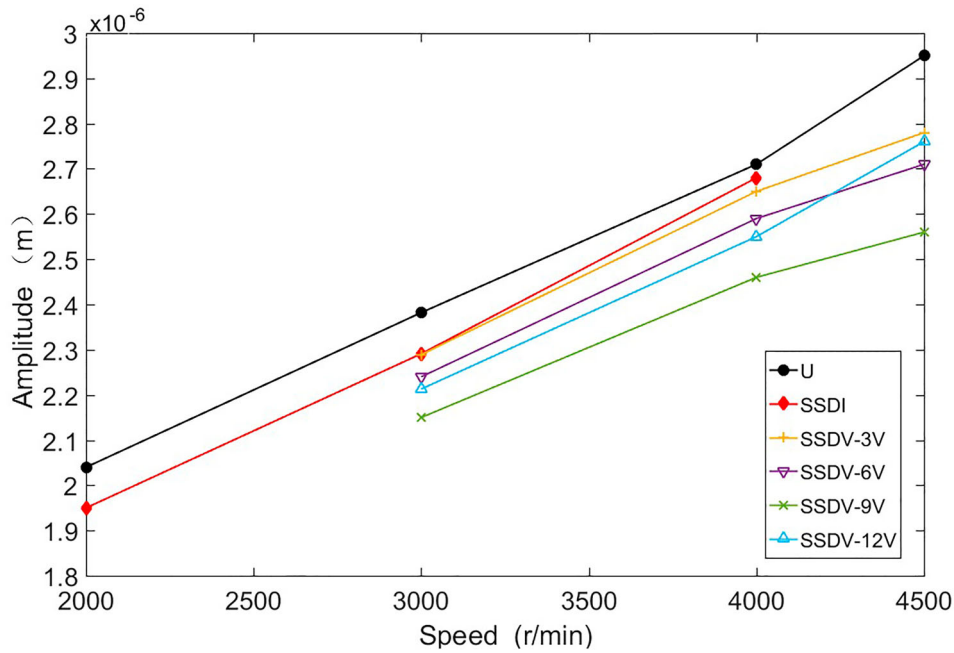


Figure 14. Vibration effect comparison at different rotating speeds.

with self-powered SSDI, it has a great degree of vibration reduction performance. These phenomena are the same as those in the simulation, and also confirm the feasibility of the designed circuit and the selected parameters. But it is reminded that vibration control performance using self-powered SSD circuit in experimental results may not be so obvious as desired. Some possible reasons are summarized:

- (1) The designed rotating spindle has weak vibration amplitude at μm scale. It is easier to observe more visible vibration control performance in the environment with relatively stronger vibration.
- (2) Efficiency of electromechanical conversion of piezoelectric stack is lower than widely utilized layered PZT patch.

Despite that, it can be still considered as feasible experimental support for our analysis and simulation results without loss of reliability of conclusion, and provide a guiding platform for semi-active control scheme used for motorized spindle. In the future, additional studies are required to further improve energy conversion efficiency.

5. Conclusion

In this study, the SSD technique is introduced into vibration control of motorized spindle and a self-powered SSDV circuit is proposed. This is based on a slight modification of SSDI circuit, and their mechanisms and performances are analyzed and compared. Subsequently, a MATLAB/Simulink electromechanical simulation model and experimental rotor-bearing

system were built to verify our analysis. The main conclusions can be summed up:

- (1) The control effects of SSDV and SSDI were compared based on the output voltage and the energy converted, and the simulation results show that SSDV is more effective than SSDI in energy conversion.
- (2) The experimental results reveal that self-powered SSDV can effectively suppress the eccentric vibration of the motorized spindle's rotor at a constant rotating speed, and it shows a better control effect than self-powered SSDI.
- (3) In the experiment, when rotating speed changes within a certain range, self-powered SSDV can always maintain the effective vibration control performance while self-powered SSDI may induce the loss of the performance. Further experimental results suggest that when the supplied voltage of self-powered SSDV is suitably selected, the suppression of the vibration amplitude of the spindle's rotor-bearing system can be enhanced correspondingly.

In summary, the self-powered SSDV circuit presented has been verified on the spindle test bench in this paper. This study certainly provides a novel way of suppressing vibration of the motorized spindle rotor-bearing system and can be used for semi-active vibration control problems of other rotating machinery. In the future, based on this work, more advanced SSD approaches like self-adaptive voltage sources and the negative capacitance can be designed and used to enhance the performance of vibration control for motorized spindles.

Disclosure statement

No potential conflict of interest was reported by the author(s).

Funding

This work was supported by the National Key Research and Development Program of China [grant number 2018YFB2000 500] and the Graduate Research and Innovation Foundation of Chongqing, China [grant number CYS21006].

ORCID

Likang Zheng  <http://orcid.org/0000-0001-8442-4684>

Ye He  <http://orcid.org/0000-0002-4457-3877>

Xiaolan Chen  <http://orcid.org/0000-0001-9428-4996>

References

- [1] Dalela S, Balaji PS, Jena DP. A review on application of mechanical metamaterials for vibration control. *Mech Adv Mater Struct.* 2021. DOI:10.1080/15376494.2021.1892244
- [2] Bendine K, Boukhoulda FB, Haddag B, et al. Active vibration control of composite plate with optimal placement of piezoelectric patches. *Mech Adv Mater Struct.* 2019;26(4):341–349. DOI:10.1080/15376494.2017.1387324.
- [3] Ding H, Zhao J. Dynamic characteristic analysis of replenishing/leaking parallel valve control systems. *Automatika.* 2017;58(2):182–194. DOI:10.1080/00051144.2017.1386750.
- [4] Mohan E, Natarajan U. Experimental investigation on boring tool vibration control using MR fluid damper. *J Adv Manuf Tech.* 2016;15(1):13–25. DOI:10.1142/S0219686716500025.
- [5] Song G, Ma N, Li HN. Applications of shape memory alloys in civil structures. *Eng Struct.* 2006;28(9):1266–1274. DOI:10.1016/j.engstruct.2005.12.010.
- [6] Ahmad I, Abdurraqueeb AM. H infinity control design with feed-forward compensator for hysteresis compensation in piezoelectric actuators. *Automatika.* 2016;57(3):691–702. DOI:10.7305/automatika.2017.02.1786.
- [7] Song G, Sethi V, Li HN. Vibration control of civil structures using piezoceramic smart materials: a review. *Eng Struct.* 2006;28(11):1513–1524. DOI:10.1016/j.engstruct.2006.02.002.
- [8] Hagood NW, Vonflotow A. Damping of structural vibrations with piezoelectric materials and passive electrical networks. *J Sound Vib.* 1991;146(2):243–268. DOI:10.1016/0022-460X(91)90762-9.
- [9] Sapra G, Sharma M, Vig R, et al. Multiwalled carbon nanotube film composite for active vibration control of cantilevered beam. *IEEE Sens J.* 2019;19(7):2466–2473. DOI:10.1109/JSEN.2018.2889651.
- [10] Sabatini M, Palmerini G, Gasbarri P. Synergetic approach in attitude control of very flexible satellites by means of thrusters and PZT devices. *Aerosp Sci Technol.* 2020;96:105541. DOI:10.1016/j.ast.2019.105541.
- [11] Yan B, Wang K, Hu Z, et al. Shunt damping vibration control technology: a review. *Appl Sci Basel.* 2017;7(5):494. DOI:10.3390/app7050494.
- [12] Mokrani B, Bastaitis R, Horodincea M, et al. Parallel piezoelectric shunt damping of rotationally periodic structures. *Adv Mater, Sci, Eng.* 2015;2015:162782. DOI:10.1155/2015/162782.
- [13] Toftekaer JF, Benjeddou A, Hogsberg J. General numerical implementation of a new piezoelectric shunt tuning method based on the effective electromechanical coupling coefficient. *Mech Adv Mater Struct.* 2020;27(22):1908–1922. DOI:10.1080/15376494.2018.1549297.
- [14] Hogsberg J. Vibration control by piezoelectric proof-mass absorber with resistive-inductive shunt. *Mech Adv Mater Struct.* 2021;28(2):141–153. DOI:10.1080/15376494.2018.1551587.
- [15] Niederberger D, Fleming A, Moheimani SOR, et al. Adaptive multi-mode resonant piezoelectric shunt damping. *Smart Mater Struct.* 2004;13(5):1025–1035. DOI:10.1088/0964-1726/13/5/007.
- [16] Krishnamoorthy SG, Skiedraite I. Attenuation of micro-vibrations by varying the resonance extremity of a transitional composite structure. *Mech Adv Mater Struct.* 2020. DOI:10.1080/15376494.2020.1716416
- [17] Eltamaly A, Addoweesh K. A novel self-power SSHI circuit for piezoelectric energy harvester. *IEEE Trans Power Electron.* 2017;32(10):7663–7673. DOI:10.1109/TPEL.2016.2636903.
- [18] Liu W, Badel A, Formosa F, et al. A comprehensive analysis and modeling of the self-powered synchronous switching harvesting circuit with electronic breakers. *IEEE Trans Ind Electron.* 2018;65(5):3899–3909. DOI:10.1109/TIE.2017.2762640.
- [19] Wu YG, Li L, Fan Y, et al. Design of dry friction and piezoelectric hybrid ring dampers for integrally bladed disks based on complex nonlinear modes. *Comput Struct.* 2020;233:106237. DOI:10.1016/j.compstruc.2020.106237.
- [20] Clark WW. Vibration control with state-switched piezoelectric material. *J Intel Mat Syst Str.* 2000;11(4):263–271. DOI:10.1106/18CE-77K4-DYMG-RKBB.
- [21] Richard C. Semi-passive damping using continuous switching of a piezoelectric device. *Smart Mater Struct.* 1999;3672:104–111. DOI:10.1117/12.349773.
- [22] Richard C. Enhanced semi-passive damping using continuous switching of a piezoelectric device on an inductor. *Smart Mater Struct.* 2000;3989:104–111. DOI:10.1117/12.384569.
- [23] Corr LR, Clark WW. Comparison of low-frequency piezoelectric switching shunt techniques for structural damping. *Smart Mater Struct.* 2002;11(3):370–376. DOI:10.1088/0964-1726/11/3/307.
- [24] Petit L, Lefeuvre E, Richard C, et al. A broadband semi passive piezoelectric technique for structural damping. *Smart Mater Struct.* 2004;5386:414–425. DOI:10.1117/12.532716.
- [25] Lefeuvre E, Badel A, Petit L. Semi passive piezoelectric structural damping by synchronized switching on voltage sources. *J Intel Mat Syst Str.* 2006;17(8–9):653–660. DOI:10.1177/1045389X06055810.
- [26] Badel A, Sebald G, Guyomar D. Piezoelectric vibration control by synchronized switching on adaptive voltage sources: towards wideband semi-active damping. *J Acoust Soc Am.* 2006;119(5):2815–2825. DOI:10.1121/1.2184149.
- [27] Lallart M, Badel A, Guyomar D. Nonlinear semi-active damping using constant or adaptive voltage sources: a stability analysis. *J Intel Mat Syst Str.* 2008;19(10):1131–1142. DOI:10.1177/1045389X07083612.
- [28] Ji H, Qiu J, Cheng J, et al. Application of a negative capacitance circuit in synchronized switch damping techniques for vibration suppression. *J Vib Acoust.* 2011;133(4):041015. DOI:10.1115/1.4003146.

- [29] Qureshi EM, Shen X, Chang L. An autonomous synchronized switch damping on inductance and negative capacitance for piezoelectric broadband vibration suppression. *Int J Aeronaut Space*. 2016;17(4):501–517. DOI:10.5139/IJASS.2016.17.4.501.
- [30] Silva TMP, Junior CDM. Energy analysis of semi-passive control for an aeroelastic plate-like wing using shunted piezoelectric materials. *J Intel Mat Syst Str*. 2016;27(19):2599–2615. DOI:10.1177/1045389X16635842.
- [31] Shen H, Qiu J, Ji H, et al. A low-power circuit for piezoelectric vibration control by synchronized switching on voltage sources. *Sensor Actuat A Phys*. 2010;161(1-2):245–255. DOI:10.1016/j.sna.2010.04.012.
- [32] Bao B, Tang W. Semi-active vibration control featuring a self-sensing SSDV approach. *Measurement*. 2017;104:192–203. DOI:10.1016/j.measurement.2017.03.018.
- [33] Tang W, Wang L, Ren Y, et al. Design and experimental analysis of self-sensing SSDNC technique for semi-active vibration control. *Smart Mater Struct*. 2018;27(8):085028. DOI:10.1088/1361-665X/aad0b9.
- [34] Ji H, Guo Y, Qiu J, et al. A new design of unsymmetrical shunt circuit with negative capacitance for enhanced vibration control. *Mech Syst Signal Pr*. 2021;155:107576. DOI:10.1016/j.ymssp.2020.107576.
- [35] He Y, Chen X, Liu Z, et al. Piezoelectric self-sensing actuator for active vibration control of motorized spindle based on adaptive signal separation. *Smart Mater Struct*. 2018;27(6):065011. DOI:10.1088/1361-665X/aabbf4.
- [36] Ogun P, Jackson M. Active vibration control and real-time cutter path modification in rotary wood planing. *Mechatronics*. 2017;46:21–31. DOI:10.1016/j.mechatronics.2017.06.007.
- [37] Albertelli P, Elmas S, Jackson MR, et al. Active spindle system for a rotary planing machine. *Int J Adv Manuf Tech*. 2012;63(9–12):1021–1034. DOI:10.1007/s00170-012-3983-9.
- [38] He Y, Chen X, Liu Z, et al. Active vibration control of motorized spindle based on mixed H_∞ /Kalman filter robust state feedback control. *J Vib Control*. 2019;25(6):1279–1293. DOI:10.1177/1077546318820935.
- [39] Zheng L, Wang Z, Zhao Z, et al. Research of bearing fault diagnosis method based on multi-layer extreme learning machine optimized by novel ant lion algorithm. *IEEE Access*. 2019;7:89845–89856. DOI:10.1109/ACCESS.2019.2926348.
- [40] Zheng L, He Y, Chen X. Research on a fault diagnosis method for rolling bearing based on improved multi-scale range entropy and hierarchical prototype. *Meas Sci Technol*. 2021;32(9):095003. DOI:10.1088/1361-6501/abfbaa.
- [41] Yuan M, Cao ZP, Luo J, et al. Recent developments of acoustic energy harvesting: a review. *Micromachines*. 2019;10(1):48. DOI:10.3390/mi10010048.
- [42] Li B, You H. Experimental study on self-powered synchronized switch harvesting on inductor circuits for multiple piezoelectric plates in acoustic energy harvesting. *J Intel Mat Syst Str*. 2015;26(13). DOI:10.1177/1045389X14566523.